Radar Fall Detectors: A Comparison

Baris Erol[a], Moeness Amin[a], Fauzia Ahmad[a*], and Boualem Boashash[b]

[a]Center for Advanced Communication, Villanova University, Villanova, PA 19085, USA
[b]Department of Electrical Engineering, College of Engineering, Qatar University, Doha, Qatar

ABSTRACT

Falls are a major cause of accidents in elderly people. Even simple falls can lead to severe injuries, and sometimes result in death. Doppler fall detection has drawn much attention in recent years. Micro-Doppler signatures play an important role for the Doppler-based radar systems. Numerous studies have demonstrated the offerings of micro-Doppler characteristics for fall detection. In this respect, a plethora of micro-Doppler signature features have been proposed, including those stemming from speech recognition and wavelet decomposition. In this work, we consider four different sets of features for fall detection. These can be categorized as spectrogram based features, wavelet based features, mel-frequency cepstrum coefficients, and power burst curve features. Support vector machine is employed as the classifier. Performance of the respective fall detectors is investigated using real data obtained with the same radar operating resources and under identical sensing conditions. For the considered data, the spectrogram based feature set is shown to provide superior fall detection performance.

Keywords: Fall Detection, micro-Doppler signatures, cepstrum, support vector machine, wavelets

1. INTRODUCTION

Falls are a major cause of fatal and non-fatal injuries in people aged 65 years and older. Prompt assistance after a fall can be instrumental in reducing health-related complications. Long periods of remaining on the floor can lead to hypothermia, dehydration, bronchopneumonia, and pressure sores in the elderly,[1,2] which can impede their recovery from an injury-causing fall. A longer recovery time implies an extended hospital stay, which can not only render the elderly more vulnerable to disease, but also add significant financial burden on the elderly family. As such, fall detection systems have been identified as a major innovation opportunity to enable self-dependent living and provide an improved quality of life for the elderly population.[3]

Recently, different types of fall detection systems have been proposed in the literature.[4,5] These detectors range from wearable, such as accelerometers and push button devices, to non-wearable technologies; the most common example of the latter being video cameras.[6] Wearable devices either require user activation or they need to be carried in the same fixed position for reliable performance. Camera systems suffer from privacy concerns, and provide degraded performance under occlusion and low lighting conditions.[7] In this work, we focus on radar fall detectors, which belong to the non-wearable category. Radar attributes, such as non-obstructive illumination, non-intrusive sensing, insensitivity to lighting conditions, and privacy preservation, have brought RF sensing to the forefront of fall detection modalities in competition with cameras and wearable devices.

Human motions generate radar returns, which represent non-stationary Doppler and micro-Doppler signals.[8-13] In assisted living applications, time-frequency (TF) representations have been employed for characterization of these signals.[14-18] Typically, a feature-based classification approach is used for fall detection, wherein features are extracted from the TF representations of the radar returns and applied to a classifier. A variety of feature sets have been proposed: a) Spectrogram features[14] capturing the physical characteristics of human motions; (b) Mel-frequency cepstrum coefficients (MFCCs) (originating from speech recognition) extracted from the TF representations;[15] (c) Wavelet transform (WT) based features;[16] and (d) Power burst curve (PBC).[17] Each feature set to date has been tested for fall detection using different radar operating resources and under different sensing conditions, rendering it difficult to compare and contrast their performances. Operating resources of the radar and the sensing conditions impact the resolution and quality of the Doppler and micro-Doppler signatures. Further, the various feature sets have been evaluated in the literature using different sizes of the testing and training data, which directly affect the classification rates. In this work, we aim to the compare the fall detection

* Corresponding author; fauzia.ahmad@villanova.edu

performance of the aforementioned four feature sets using same radar operating resources, testing/training data, and under identical sensing conditions.

The paper is organized as follows. In Section 2, we briefly review the radar signal model and describe the four considered feature sets. Performance evaluations of the various feature sets using real data measurements are provided in Section 3, while conclusions are drawn in Section 4.

2. SIGNAL MODEL AND FEATURE SETS

2.1 Signal model

For a continuous-wave (CW) radar, the baseband radar return from a moving point target can be expressed as,

$$x(t) = \rho(t)\exp(-j\phi(t)), \tag{1}$$

where $\rho(t)$ and $\phi(t)$ are the time-varying amplitude and phase of the return, respectively. The phase contains the information about the motion of the target and the derivative of the phase provides the corresponding Doppler frequency. The returns from more complex targets, such as humans, can be expressed as the sum of returns from multiple point scatterers comprising the target extent. In such cases, the corresponding Doppler signature is the superposition of the various component Doppler frequencies.

Since the Doppler radar return, $x(t)$, from the human is non-stationary, joint variable representation is a natural tool for revealing the local signal behavior and depicting its time-varying Doppler signatures with enhanced energy concentration.

In this paper, we work with the discrete version of the baseband radar return in (1), given by

$$x(n) = x(t)|_{t=nT_s}, n = 0, 1, \ldots, N-1. \tag{2}$$

where T_s is the sampling period.

2.2 Spectrogram Based Features

Spectrogram is a commonly used technique for TF analysis.[19] The spectrogram $SPEC(n,k)$ is defined as

$$SPEC(n,k) = \left| \sum_{m=0}^{N-1} x(n+m)h(m)e^{-j2\pi mk/N} \right|^2, \tag{3}$$

where $h(m)$ is a window function that can affect both time and frequency resolutions. Fig. 1 shows the spectrograms corresponding to four different human motions. A Hanning window of length 128 samples was used to generate the spectrograms. It can be readily seen that each motion has its own unique signature. This uniqueness is reasonable because the speed and kinematics of the various motions are different. Thus, extraction of features that capture the intrinsic differences between the TF signatures corresponding to various human motion articulations can aid in motion classification. In this work, three features, namely, extreme Doppler frequency, torso frequency, and the length of the event, are considered for fall detection (see Fig. 2). These features, especially the extreme Doppler frequency, have been frequently employed in the literature for fall detection in assisted living applications.[14]

2.2.1 Extreme Doppler Frequency Extraction

An energy-based thresholding algorithm is established to determine the outer envelope of the micro-Doppler signature from which the extreme Doppler frequency can be extracted. First, the energy corresponding to the slow time n is computed as

$$E_T(n) = \sum_{k=1}^{M} S(n,k)^2 \tag{4}$$

where $k = 1, 2, ..., M$ are the Doppler indices and $S(n,k)$ is the spectrogram. Next, for the slow time index n, the first frequency bin whose corresponding spectrogram value is greater than or equal to the product of a pre-determined threshold and E_T is determined. The two-step process is repeated for all $n = 1, 2, ..., N$, leading to

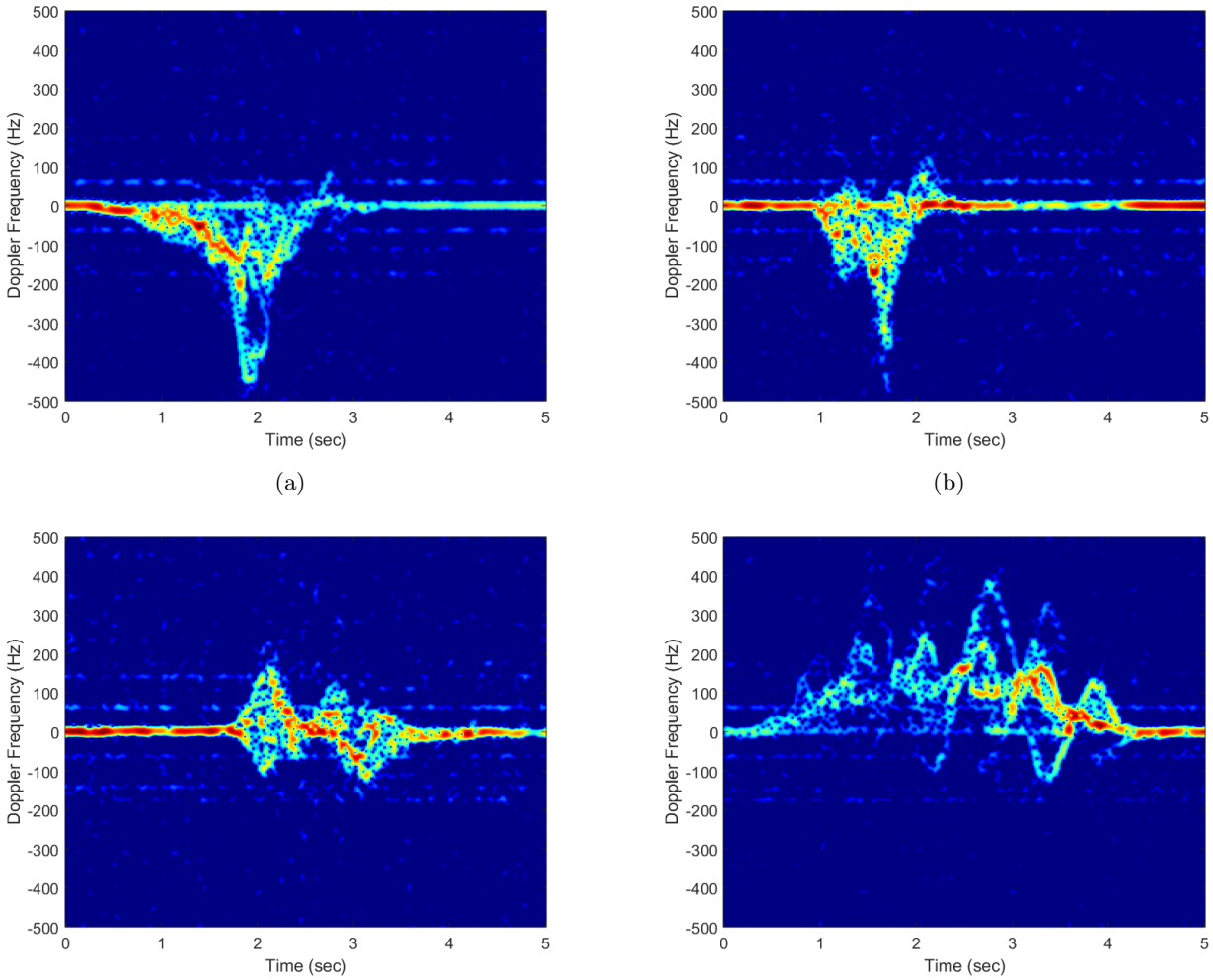

Figure 1: Spectrograms of different motions: (a) Falling (b) Sitting (c) Picking up an object (d) Walking.

extraction of the outer envelope of the signature, from which the extreme Doppler frequency can be determined. The outer envelope (red dashed curve) of a fall motion is depicted in Fig. 2. A threshold value was empirically chosen such that it provided the best separation between fall and non-fall events.

2.2.2 Torso Doppler Frequency Extraction

The larger cross-section of the torso generally results in a higher power concentration in the corresponding micro-Doppler signature. This attribute is utilized to determine the torso Doppler frequency, f_{torso}, as

$$f_{torso} = \max_n |-1/2T_s + (\lambda_n - 1)/(M-1)T_s|, \quad \lambda_n = \arg\max_k S(n,k). \tag{5}$$

The torso Doppler signature (solid black curve) for a fall motion is depicted in Fig. 2. Clearly, torso Doppler frequency has a lower value than the extreme Doppler frequency.

2.2.3 Length of the Event

This feature defines the time, in seconds, between the start and the end of an event. The length of an event can be determined by monitoring the PBC, which is defined as the summation of signal power within a specific

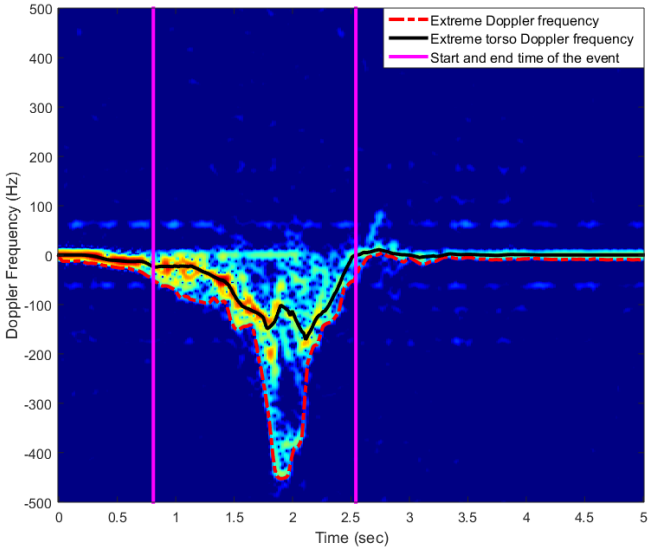

Figure 2: Spectrogram-based features

frequency band $[k_l, k_u]$.[15,20] That is,

$$PBC(n) = \sum_{k=k_l}^{k_u} |S(n,k)|^2, \quad n = 1, 2, ..., N. \tag{6}$$

In this work, k_l and k_u are chosen as the frequency indices corresponding to -50 Hz and -500 Hz, respectively. This choice was determined by an examination of the spectrograms of different motions being used for performance evaluation. The PBC corresponding to the fall signature of Fig. 1(a) is provided in Fig. 3. The start of an event is determined as the time index at which the PBC exceeds a specific threshold, while the end of the event corresponds to a later time where the PBC falls below the threshold. The threshold is typically selected to maintain sensitivity to human motion event while ensuring sufficient separation from the noise floor.[20]

2.3 Mel-Frequency Cepstrum Coefficients Features

Recently, speech recognition inspired features, such as MFCCs, have been also exploited for fall detection.[15] Mel-frequency cepstrum coefficients are generated by first filtering the signal spectrum using a filter bank defined according to the mel-scale, then taking the logarithm of the resulting mel-energy spectrum, followed by the applying the discrete cosine transform (DCT) to compute the coefficients. The mel-scale is a perceptual scale of pitches judged by listeners to be equal in distance from one another. The human ear interpretation of a pitch is determined as linearly perceived in the frequency range 0-1000 Hz, while above 1000 Hz, the scale becomes logarithmic. An approximated formula of the mel-scale is defined as

$$f_{mel} = 2595 \log_{10}(1 + \frac{f_{Hz}}{700}) \tag{7}$$

where f_{Hz} is the true frequency and f_{mel} is the mel-scale warped frequency. The resulting mel-scale filter-bank possesses narrower filters at lower frequency bands, whereas at higher frequency bands, the filter bandwidths become broader. This is because most of the energy in speech signals lies in the low frequency bands. However, this is not an optimum choice to extract MFCCs for fall detection. Further, in speech recognition, the frequency limits for mel-scale are defined as 0 and 4 kHz, with the original frequency values between 0 and 16 kHz. Applying these frequency limits to the fall detection problem will create empty filters as the frequency band of interest for

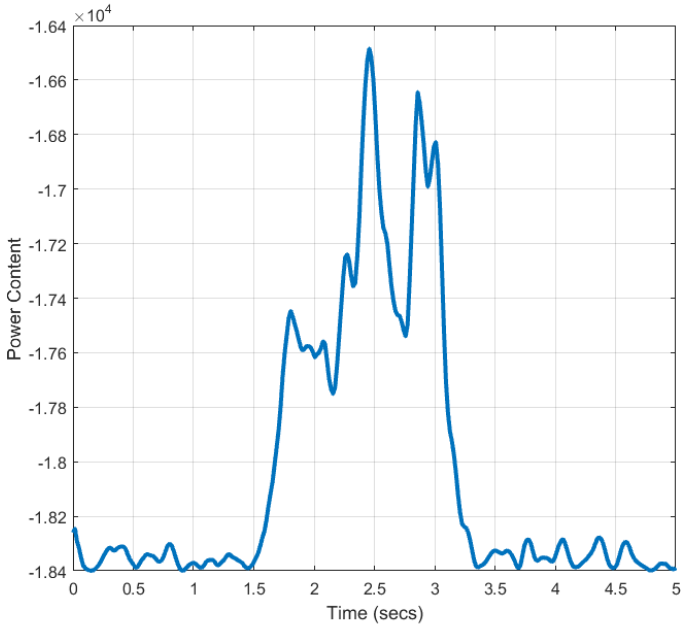

Figure 3: Power burst curve corresponding to Fig. 1(a).

the considered human motions in this work is [-500, 500] Hz. Furthermore, mel-scale filter bank does not span the negative frequencies, which are often encountered in fall detection depending on the direction of the motion realtive to the radar. To address these issues,we redefined the limits of the mel-scale function as -500 Hz and 500 Hz to span the whole Doppler spectrum. An example of the redefined filter-bank is depicted in Fig. 4(a). It can be clearly seen that the filter bank focuses on the negative frequency bands as well as positive frequency bands and covers the entire spectrum of interest.

For each slow time index n, $S(n, k)$ passes through the filter bank, followed by computation of the logarithm

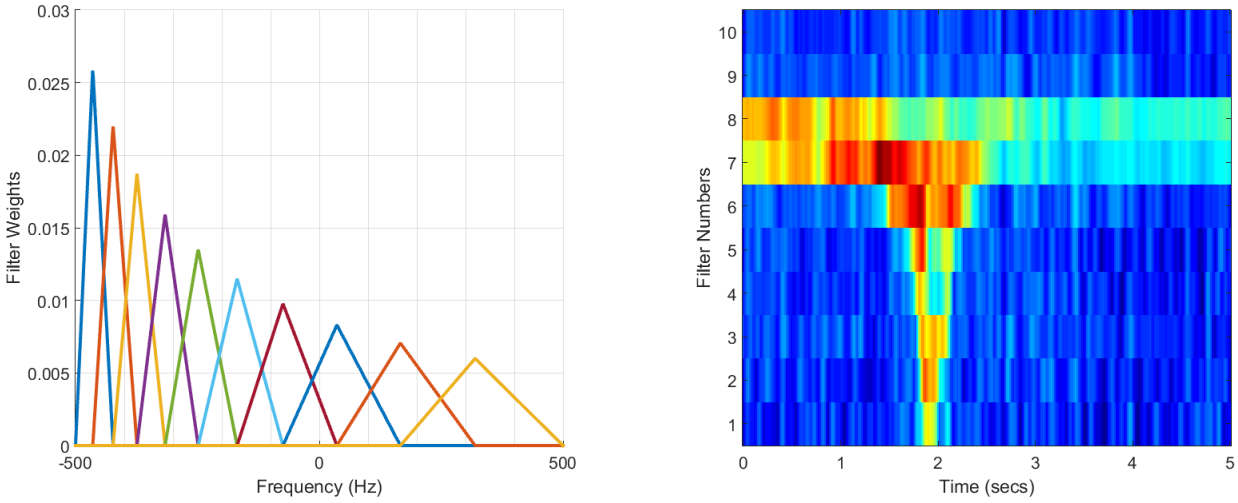

(a) (b)

Figure 4: (a) Mel-scale filterbank (b) Log-energy output.

of the outputs. Mathematically, the "log-energy" output of the mth filter, $X_m(n)$, can be expressed as

$$X_m(n) = \log_{10}(\sum_{k=1}^{K-1} |S(n,k)|H_m(k)), \quad m = 1, 2, ..., M, \tag{8}$$

where M is the number of filters, $H_m(k)$ is the mth filter response. The log-energy output corresponding to spectrogram of Fig. 1(a) is depicted in Fig. 4(b). In the final step of the algorithm, the DCT is applied to the log-energy output to compute the MFCCs.

2.4 Wavelet Features

The WT of a signal $x(n)$ is defined as

$$X(i,a) = \frac{1}{\sqrt{a}} \sum_n x(n) f^*\big(\frac{i-n}{a}\big) \tag{9}$$

where f^* is the wavelet function, a is the scale factor, i denotes the translation, and $1/\sqrt{a}$ is the energy normalization factor.

Depending on the scale a, the wavelet function can be represented by a pair of low and high pass filters. The WT can be also efficiently computed as Discrete Stationary Wavelet Transform (SWT). SWT is an online process that transforms the incoming data sequentially through successive applications of the filters.[16] Fig. 5 depicts the SWT outputs, $D_i(n), i = 1, 2, ..., 6$, corresponding to the real and imaginary parts of the radar return of the fall in Fig. 1(a). The fall occured between 0.89 and 2.6 s. Reverse biorthogonal 3.3 (rbio3.3) is used as the wavelet function which was shown to yield better classification performance for fall detection over other types of wavelet functions.[16] We observe from Fig. 5 that the SWT outputs $D_2(n)$ and $D_3(n)$ capture most of signal energy. Therefore, we only focus on $D_2(n)$ and $D_3(n)$ for fall detection.

The energy between the start and the end of an event can be expressed as

$$E_i = \sum_n (w(n)D_i(n))^2, \quad i = 2, 3 \tag{10}$$

where the summation is over values of n within the length of the event and $w(k)$ is a Hanning window function. The energy values, E_i, are computed for both real and imaginary parts of the data and serve as features used for classification.

2.5 Power Burst Curve Features

Power burst curves have also been used as features for fall detection.[17] The PBC has been defined in Section 2.2.3. The entire PBC values over slow time are used as the feature vector for classification.

3. EXPERIMENTAL RESULTS

Experiments were performed in the Radar Imaging Lab at the Center for Advanced Communications, Villanova University. A 24 GHz radar system, SDR-KIT 2500B by Ancortek, Inc., was used in the CW mode for data collections. Four different human motions were considered: falling, sitting, picking an object from the floor, and walking. Each motion signal was recorded for 15 seconds at a sampling rate of 1 kHz. Four different human subjects, with heights ranging from 1.73 m to 1.90 m and weighing between 70 kg to 95 kg, were asked to repeat the four activities several times. A total of 93 experiments were conducted, with 30 corresponding to falling and the remaining 63 experiments related to the three considered non-fall motions. The four aforementioned feature sets were extracted. A support vector machine (SVM) classifier with a radial basis kernel function was employed. 60% of the recorded signals were used for training the classifier, whereas the remaining 40% were used for testing. The allocation of data measurements to training and testing sets was carried out in a random fashion. As such, 1000 Monte Carlo trials with a different random allocation for each run were performed to evaluate the fall detection performance of the four considered feature sets.

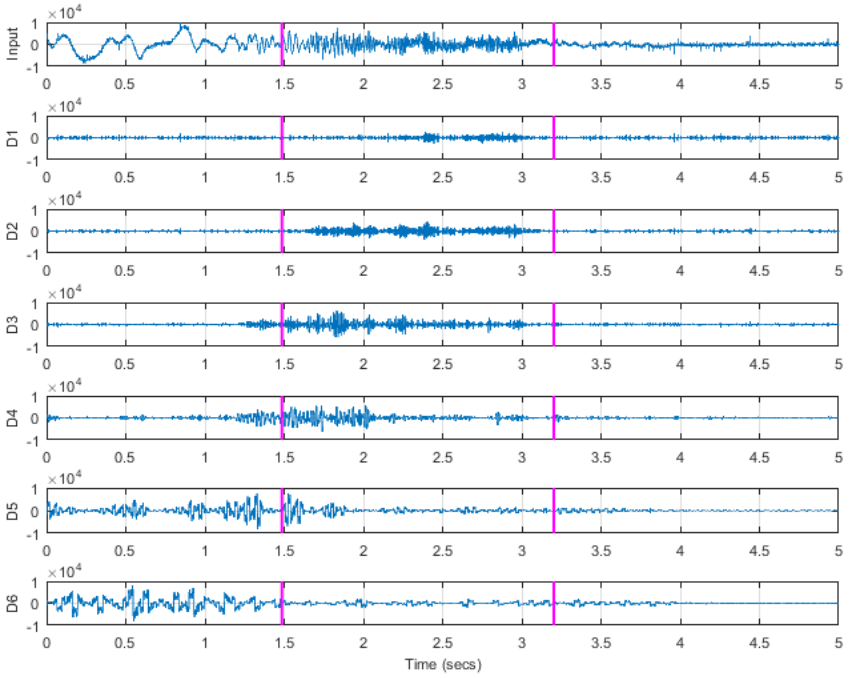

(a)

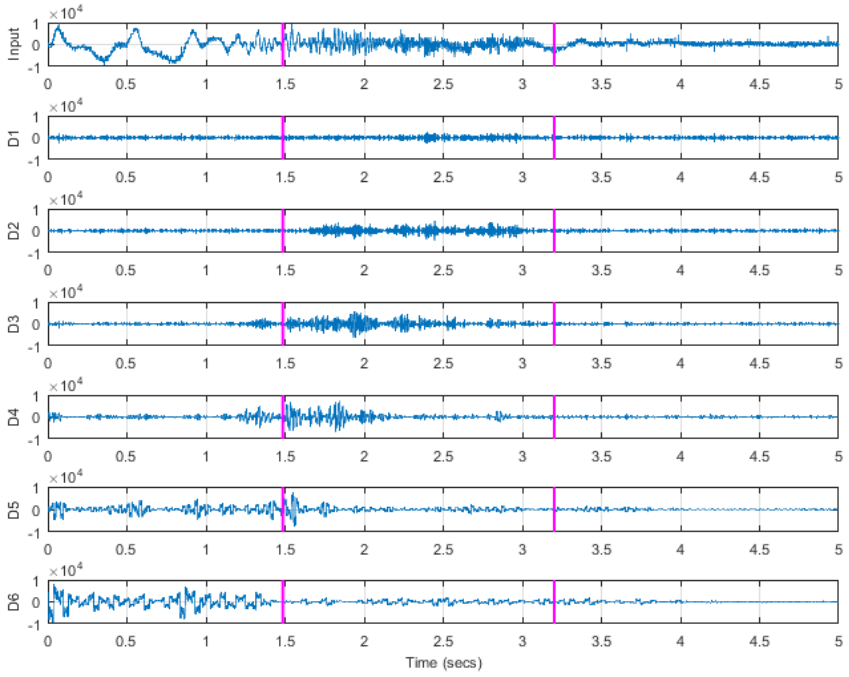

(b)

Figure 5: Wavelet decomposition of the (a) real and (b) imaginary part of the Doppler signal

Confusion matrices for the four feature sets are provided in Tables 1 through 4. The average classification rates for spectrogram-based, MFCCs, wavelet-based, and PBC feature sets are determined to be 93%, 90%, 91.5%, and 88.5%, respectively. The spectrogram-based and wavelet-based feature sets provide the lowest false alarm rates, while PBC produces the highest. Spectrogram-based features produce the lowest number of missed detections, whereas both wavelet-based and MFCC features have the highest missed detection rate.

Table 1: Confusion matrix for spectrogram features

Activity-Class	Fall	Non-Fall
Fall	0.92	0.08
Non-Fall	0.06	0.94

Table 2: Confusion matrix for MFCCs

Activity-Class	Fall	Non-Fall
Fall	0.89	0.11
Non-Fall	0.09	0.91

Table 3: Confusion matrix for wavelet features

Activity-Class	Fall	Non-Fall
Fall	0.89	0.11
Non-Fall	0.06	0.94

Table 4: Confusion matrix for PBC

Activity-Class	Fall	Non-Fall
Fall	0.90	0.10
Non-Fall	0.13	0.87

In Fig. 6, the impact of the training data size is analyzed for each candidate feature set. It can be clearly seen that both spectrogram-based and wavelet-based features are robust to the training data size. Both MFCCs and PBC features provide low classification rates for smaller training data sizes. This can be attributed to the high dimensionality of the associated feature space.

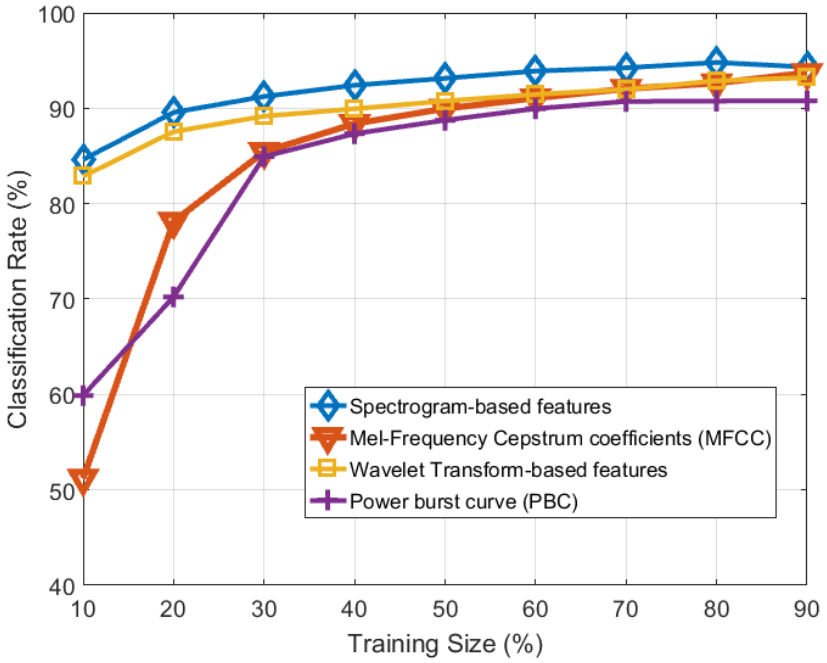

Figure 6: The impact of the training data size on classification rate

4. CONCLUSION

In this paper, we compared the fall detection performance of spectrogram, MFCC, wavelet, and PBC feature sets proposed in the literature under the same radar operating resources and sensing conditions. Real data measurements corresponding to four different human motions, namely, falling, sitting, picking up an object from the floor, and walking, were considered. Employing SVM as the classifier, we demonstrated that, for the data considered, the spectrogram-based features outperform the other feature sets in terms of classification, false alarm, and missed detection rates.

ACKNOWLEDGMENTS

This paper is made possible by NPRP Grant # NPRP 6-680-2-282 from the Qatar National Research Fund (a member of Qatar Foundation). The statements made herein are solely the responsibility of the authors.

REFERENCES

1. L. Z. Rubenstein and K. R. Josephson, "The epidemiology of falls and syncope," *Clin. Geriatr. Med.* **18**(2), pp. 141–158, 2002.
2. M. E. Tinetti, W. L. Liu, and E. B. Claus, "Predictors and prognosis of inability to get up after falls among elderly persons," *JAMA* **269**(1), pp. 65–70, 1993.
3. *Health Innovation Frontiers: Untapped Market Opportunities for the 50+.* http://www.aarp.org/content/dam/aarp/home-and-family/personal-technology/2013-08/Health-Innovation-Frontiers-Untapped-Market-Opportunities-for-50%2B-Full-Report-AARP.pdf., 2013.
4. F. Ahmad, A. E. Cetin, K. C. Ho, and J. E. Nelson, "Special section on signal processing for assisted living," *IEEE Sig. Process. Mag.* **33**(2), pp. 25–94, 2016.
5. F. Ahmad, R. M. Narayanan, and D. Schreurs, "Special issue on application of radar to remote patient monitoring and eldercare," *IET Radar, Sonar, and Navig.* **9**(2), pp. 115–190, 2015.
6. R. Igual, C. Medrano, and I. Plaza, "Challenges, issues and trends in fall detection systems," *Biomed Eng Online* **12**(66), p. 66, 2013.
7. *Center for Diease Control and Prevention, Important facts about falls.* http://www.cdc.gov/homeandrecreationalsafety/falls/adultfalls.html., 2015.
8. P. V. Dorp and F. C. A. Groen, "Feature-based human motion parameter estimation with radar," *Sonar Navigation IET Radar* **2**(2), pp. 135–145, 2008.
9. Y. Kim, S. Ha, and J. Kwon, "Human detection using doppler radar based on physical characteristics of targets," *IEEE Geoscience and Remote Sensing Letters* **12**(2), pp. 289–293, 2015.
10. V. C. Chen, *The micro-Doppler effect in radar*, Artech House, 2011.
11. B. G. Mobasseri and M. G. Amin, "A time-frequency classifier for human gait recognition," *Proc. SPIE* **73062**, 2009.
12. C. Karabacak, S. Z. Gurbuz, A. C. Gurbuz, M. B. Guldogan, G. Hendeby, and F. Gustafsson, "Knowledge exploitation for human micro-doppler classification," *IEEE Geoscience and Remote Sensing Letters* **12**(10), pp. 2125–2129, 2015.
13. J. Lei and C. Lu, "Target classification based on micro-doppler signatures," *in IEEE International Radar Conference* , pp. 179–183, 2005.
14. Q. Wu, Y. D. Zhang, W. Tao, and M. G. Amin, "Radar-based fall detection based on doppler time-frequency signatures for assisted living," *Sonar Navigation IET Radar* **9**(2), pp. 164–172, 2015.
15. L. Liu, M. Popescuand, M. Skubicand, M. Rantzand, T. Yardibi, and P. Cuddihy, "Automatic fall detection based on doppler radar motion signature," *in 2011 5th International Conference on Pervasive Computing Technologies for Healthcare (PervasiveHealth)* , pp. 222–225, 2011.
16. B. Y. Su, K. C. Ho, M. J. Rantz, and M. Skubic, "Doppler radar fall activity detection using the wavelet transform," *IEEE Transactions on Biomedical Engineering* **62**(3), pp. 865–875, 2015.
17. J. Hong, S. Tomii, and T. Ohtsuki, "Cooperative fall detection using doppler radar and array sensor," *in 2013 IEEE 24th International Symposium on Personal Indoor and Mobile Radio Communications* , pp. 3492–3496, 2013.
18. M. G. Amin, Y. D. Zhang, F. Ahmad, and K. C. Ho, "Radar signal processing for elderly fall detection: The future for in-home monitoring," *IEEE Signal Processing Magazine* **33**(2), pp. 71–80, 2016.
19. B. Boashash, *Time-Frequency Signal Analysis and Processing: A Comprehensive Reference*, Elsevier, Oxford, 2003.
20. L. R. Rivera, E. Ulmer, Y. D. Zhang, W. Tao, and M. G. Amin, "Radar-based fall detection exploiting time-frequency features," *in 2014 IEEE China Summit International Conference on Signal and Information Processing (ChinaSIP)* , pp. 713–717, 2014.